AGU PUBLICATIONS

JGR

Journal of Geophysical Research: Earth Surface

RESEARCH ARTICLE
10.1002/2016JF003937

Key Points:
- Gradual development of ice streams causes large ice sheets to be more sensitive to external forcing
- An upward shift in the ELA enhances ice stream discharge and causes rapid deglaciation
- Discharge and surface melting are entangled processes that are both critical to rapid deglaciation

Supporting Information:
- Supporting Information S1

Correspondence to:
A. A. Robel,
robel@caltech.edu

Citation:
Robel, A. A., and E. Tziperman (2016), The role of ice stream dynamics in deglaciation, *J. Geophys. Res. Earth Surf.*, *121*, 1540–1554, doi:10.1002/2016JF003937.

Received 3 MAY 2016
Accepted 4 AUG 2016
Accepted article online 9 AUG 2016
Published online 31 AUG 2016

The role of ice stream dynamics in deglaciation

Alexander A. Robel[1,2,3] and Eli Tziperman[1]

[1]Department of Earth and Planetary Sciences and School of Engineering and Applied Sciences, Harvard University, Cambridge, Massachusetts, USA, [2]Division of Geological and Planetary Sciences, California Institute of Technology, Pasadena, California, USA, [3]Department of the Geophysical Sciences, University of Chicago, Chicago, Illinois, USA

Abstract Since the mid-Pleistocene transition, deglaciation has occurred only after ice sheets have grown large while experiencing several precession and obliquity cycles, indicating that large ice sheets are more sensitive to Milankovitch forcing than small ice sheets are. Observations and model simulations suggest that the development of ice streams in the Laurentide Ice Sheet played an as yet unknown role in deglaciations. In this study, we propose a mechanism by which ice streams may enhance deglaciation and render large ice sheets more sensitive to Milankovitch forcing. We use an idealized configuration of the Parallel Ice Sheet Model that permits the formation of ice streams. When the ice sheet is large and ice streams are sufficiently developed, an upward shift in equilibrium line altitude, commensurate with Milankovitch forcing, results in rapid deglaciation, while the same shift applied to an ice sheet without fully formed ice streams results in continued ice sheet growth or slower deglaciation. Rapid deglaciation in ice sheets with significant streaming behavior is caused by ice stream acceleration and the attendant enhancement of calving and surface melting at low elevations. Ice stream acceleration is ultimately the result of steepening of the ice surface and increased driving stresses in ice stream onset zones, which come about due to the dependence of surface mass balance on elevation. These ice sheet simulations match the broad features of geomorphological observations and add ice stream dynamics that are missing from previous model studies of deglaciation.

1. Introduction

The 100 kyr glacial cycles that have occurred since the mid-Pleistocene transition (approximately 700 kyr before present) have been marked by rapid transitions from glacial to interglacial states [*Broecker and Van Donk*, 1970]. Milankovitch forcing is commonly believed to have paced these transitions [*Hays et al.*, 1976], likely due to nonlinear phase locking [*Hyde and Peltier*, 1987; *Gildor and Tziperman*, 2000; *Tziperman et al.*, 2006]. During glacial periods, the Laurentide Ice Sheet experiences several precession (19–23 kyr) and obliquity (41 kyr) cycles before responding with a full deglaciation only when it is large, leading to the 100 kyr glacial-interglacial period. However, rapid deglaciations of large ice sheets cannot be explained by the magnitude of Milankovitch forcing, and internal feedbacks within the Earth system likely played a dominant role in producing these rapid deglaciations. Numerous non-ice dynamic feedbacks have been suggested, including changes to the thermohaline circulation [*Broecker and Denton*, 1989], dust loading [*Peltier and Marshall*, 1995], CO_2 feedbacks [*Toggweiler*, 1999; *Stephens and Keeling*, 2000; *Gildor et al.*, 2002], and changes in sea ice cover [*Gildor and Tziperman*, 2000; *Li et al.*, 2005].

Though these climate feedbacks have been shown to amplify deglaciation once it has already begun, they have had more limited success in explaining the exact timing and initial rate of deglaciation. The 100 kyr time scale of glacial cycles is closer to the time scale associated with the growth of ice sheets; therefore, glaciological feedbacks are often also invoked as a trigger of deglaciation. This includes the height-mass balance feedback [*Weertman*, 1961] and lagged bedrock rebound [*Oerlemans*, 1980; *Pollard*, 1982; *Abe-Ouchi et al.*, 2013]. *Pollard* [1982] also suggested that changes in calving at the ice sheet margins may help explain the rate of Laurentide deglaciation and the 100 kyr periodicity of glacial cycles. Models based on such feedbacks sometimes reproduce fast deglaciations but have highly parameterized certain aspects of ice sheet dynamics.

Calving at the ice sheet margin [*Pollard*, 1982], meltwater production in temperate basal ice [*Marshall and Clark*, 2002], and sliding over soft subglacial till [*Clark et al.*, 1999; *Huybers and Tziperman*, 2008] have all been proposed as necessary conditions for deglaciation of an ice sheet. All of these processes are associated with ice streaming and indicate that the gradual development of ice streams under temperate bed conditions

raises the potential for rapid ice sheet collapse. Observations indicate that many such ice streams were present and were sources of variability within the Laurentide and Eurasian ice sheets [*Stokes and Clark*, 2001], as well as in the modern Antarctic and Greenland Ice Sheets [*Retzlaff and Bentley*, 1993; *Payne*, 1999; *Catania et al.*, 2012; *Bougamont et al.*, 2015]. In particular, millennial-scale glacial climate variability, such as Heinrich events, points to ice streams as capable of producing rapid ice sheet change, even in the absence of Milankovitch forcing [*MacAyeal*, 1993; *Calov et al.*, 2002, 2010; *Ziemen et al.*, 2014; *Alvarez-Solas et al.*, 2010; *Marcott et al.*, 2011; *Alvarez-Solas et al.*, 2011]. Though observations and models generally agree that ice stream discharge was reduced near the end of the last deglaciation (approximately 9–13 kyr B.P.) [*Shaw et al.*, 2006; *Stokes and Tarasov*, 2010; *Margold et al.*, 2015], there is still disagreement over the extent to which changes in ice stream discharge flux may have played a role in the early phases of deglaciation (approximately 13–24 kyr B.P.) [*Tarasov et al.*, 2012; *Ullman et al.*, 2015; *Stokes et al.*, 2016].

Observations and coarse-resolution shallow ice models have raised new questions regarding the role of ice streams in deglaciation. This study attempts to address these questions using an ice sheet model that resolves ice streams to perform idealized simulations probing the response of an ice sheet to a prescribed upward shift in equilibrium line altitude (ELA) that corresponds to and is motivated by the effect of Milankovitch forcing on the ELA. The development of ice streams during ice sheet growth is demonstrated to result in an increased sensitivity of large ice sheets to Milankovitch forcing, leading to the observed deglaciations occurring only when the ice sheet reaches a certain threshold size. We find that forcing ice sheets by raising the ELA causes a rapid deglaciation due to an acceleration in ice stream discharge rate and, to a lesser extent, increased surface melting in ice streams. We trace the fundamental cause of the ice stream response to increasing driving stress in ice stream onset zones due to the upward shift in ELA.

Section 2 introduces the configuration of the ice sheet model and climate forcing. Section 3 describes ice sheet buildup, deglaciation, the role of ice streams in enhancing the large ice sheet sensitivity to forcing, and the robustness of the response. Sections 4 and 5 conclude by discussing the relevance to other modeling studies and observations.

2. Model Configuration

To simulate an ice sheet with the capacity to form dynamically evolving ice streams, we employ the Parallel Ice Sheet Model (PISM), an open-source 3-D thermomechanical ice sheet model. We use the hybrid force balance scheme [*Bueler and Brown*, 2009], a composite of the shallow ice and shallow shelf approximations for ice sheet flow which includes lateral viscous shear stresses. The simulations described in sections 3.1–3.5 are performed on a horizontal rectangular grid with 5 km resolution, and all simulations in this study use a quadratic vertical grid with 40–200 m resolution (see full model description in *Bueler and Brown* [2009]).

The idealized bed configuration has an axisymmetric topography, with a flat continental interior, rapidly falling away below sea level,

$$b(r) = b_0 \left[1 - \left(\frac{r}{L}\right)^8\right] \text{ meters}, \tag{1}$$

where b_0 is the height of continent, $r = \sqrt{x^2 + y^2}$ is the distance from the center of the domain, and L is the distance of the coastline from the center of the domain. The ice sheet may expand onto marine portions of the bed below sea level, where calving is permitted. All floating ice is assumed to immediately calve, and the model setup therefore does not include buttressing effects by ice shelves. In this study, we opt to focus on ice sheet dynamics upstream of the grounding line (see section 4 for discussion).

The bed is assumed to be till covered everywhere. Basal sliding over the till is governed by a Mohr-Coulomb plastic friction law [*Truffer et al.*, 2001; *Schoof*, 2006]. The yield stress of the till is

$$\tau_c = (\tan \phi)\, N_{\text{till}}, \tag{2}$$

where ϕ is a specified till friction angle and $N_{\text{till}} = N(W_{\text{till}})$ is the effective pressure at the ice-till interface, which is determined by the local till water content (W_{till}). Our idealized configuration includes prescribed regions of weak till where ice streams can form. There are 56 weak till strips, each 40 km wide, beginning at the center of the domain and radiating outward to the edge of the domain. In the weak till strips, the till friction angle is set sufficiently low ($\phi = 10°$) to permit significant basal motion when the till is saturated with meltwater.

Table 1. Prescribed Parameters Used in Model Simulations (Unless Otherwise Indicated)

Parameter	Description	Value in Sections 3.1–3.5	Value in Section 3.6
b_0	Continental height (m)	100	100
G	Geothermal heat flux (W m^{-2})	0.03	0.03
$H_{\mathrm{ELA},i}$	Initial equilibrium line altitude (m)	0	0
$H_{\mathrm{ELA},f}$	Final equilibrium line altitude (m)	600	600
H_R	Saturation elevation above ELA (m)	12	60
L	Coastline distance from domain center (m)	10^6	10^6
T_s	Sea level atmospheric temperature (°C)	−5	−5
W	Weak till strip width (km)	40	80
β	Surface mass balance gradient (yr^{-1})	0.005	0.005
Δ_{SMB}	Meridional SMB gradient (yr^{-1})	0	1.6×10^{-7}
Γ	Atmospheric lapse rate (°C km^{-1})	5	5

Elsewhere, a uniform, high till friction angle of $\phi = 80°$ is specified, which ensures that the yield stress is not achieved and there is no basal motion (even when the till is saturated with meltwater). The bed is configured in this way so that the proportion of the full simulated ice sheet margin undergoing ice streaming can be set to a level resembling that inferred from geomorphological observations of the Laurentide Ice Sheet at the Last Glacial Maximum [*Margold et al.*, 2015]. We tested an alternate bed configuration with half the number of weak till strips, each twice the width of the ice streams in our primary configuration, finding the same proportion of the margin is streaming and less than 5% difference in the simulated ice sheet volume during growth and deglaciation (Figure S2 of the supporting information). In further sensitivity studies, we found little sensitivity to the till friction angle within the weak till strips up to $\phi = 20°$, due to the role of meltwater in weakening till beneath fast-flowing ice.

The effects of changing climate forcing caused by orbital variations are represented through specified changes to the ELA, which is the elevation at which the net surface mass balance is zero. The surface mass balance (accumulation minus melting) depends on the vertical distance from the ELA ($H = h + b - H_{\mathrm{ELA}}$ where h is ice thickness, b is bed elevation, and H_{ELA} is the position of the ELA) as follows

$$M(H) = \begin{cases} \beta H & \text{if } H < H_R \\ \beta H_R & \text{if } H \geq H_R, \end{cases} \tag{3}$$

increasing linearly with ice sheet surface elevation (at a rate $\beta = 0.005$ in all simulations) until a specified saturation elevation just above the ELA (H_R), where surface mass balance is assumed to reach a constant, consistent with previous studies [*Jenson et al.*, 1996; *Cutler et al.*, 2000; *Oerlemans*, 2002; *Pollard and DeConto*, 2005]. We represent the effects of increased summer insolation and melting due to Milankovitch forcing and accompanying climate feedbacks via a spatially uniform increase in the ELA.

Sea level atmospheric temperature (T_s) is specified, and the atmospheric temperature at the ice surface decreases with ice surface elevation according to the moist adiabatic lapse rate ($\Gamma = 5$°C/km),

$$T(H) = T_s - \Gamma(H + H_{\mathrm{ELA}}). \tag{4}$$

We set a spatially uniform sea level atmospheric temperature, which we keep constant in time to focus on the impact of changing ELA. Ice sheet surface temperature partly sets the internal temperature of the ice sheet, which determines ice rheology and basal sliding through vertical heat diffusion. The results discussed in this study are not qualitatively sensitive to reasonable changes in prescribed lapse rate and sea level atmospheric temperature (see sensitivity studies in the supporting information). Geothermal heat flux is prescribed as a spatially uniform value [*Davies*, 2013]. All parameter values used in this study are specified in Table 1, and when they are varied we indicate such in the text.

3. The Sensitivity of Large Ice Sheets to Forcing

The primary goal of this study is to determine the sensitivity of an ice sheet, via ice stream activity, to an orbitally induced change in the ELA climate forcing at different stages of ice sheet development. Such changes

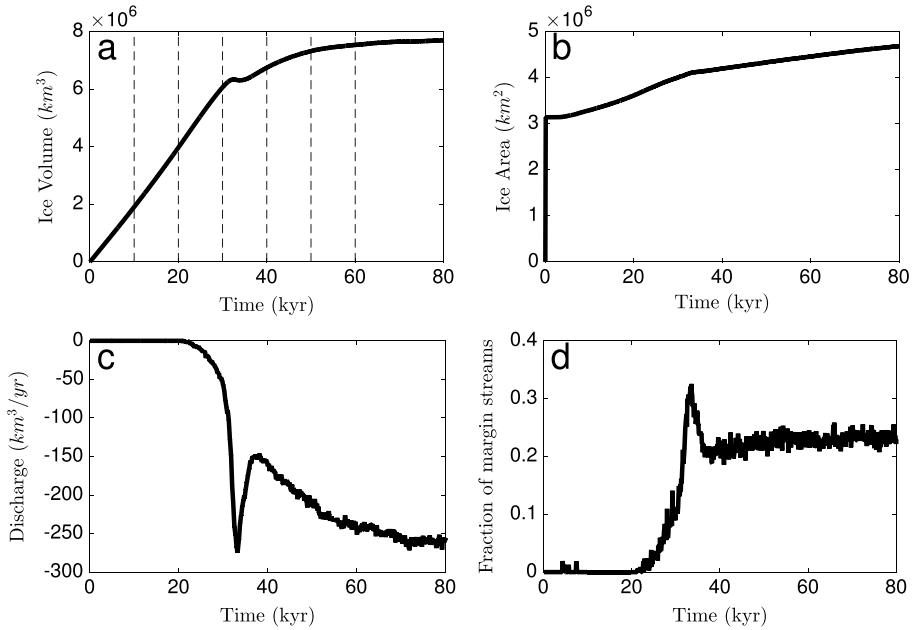

Figure 1. Evolution of important diagnostic quantities during ice sheet growth. (a) Ice sheet volume (with times of forcing in Figure 2 marked with dashed lines). (b) Ice sheet area. (c) Discharge due to calving at margin. (d) Fraction of margin in ice streams.

in ELA related to Milankovitch forcing have been deduced from a variety of observations [*Andrews et al.*, 1972; *Budd and Smith*, 1981; *Pelto*, 1992], simulated in full climate models [e.g., *Ullman et al.*, 2015] and used extensively as climate forcing parameters in ice sheet modeling studies [e.g., *Ghil and Treut*, 1981; *Oerlemans*, 2003]. We first describe the initial spin-up of the ice sheet and ice streams (section 3.1); we then show that the initial deglaciation response to step change of surface forcing occurs more dramatically with fully developed ice streams (section 3.2) and includes a significant acceleration in ice stream flux (section 3.3), leading to rapid deglaciation (section 3.4). Finally, we show (sections 3.5 and 3.6) that the results hold when the temporal structure of the forcing is more realistic and when the ice sheet is configured to more closely resemble the Laurentide Ice Sheet.

3.1. Spin-Up to Equilibrium of the Ice Sheet and Ice Streams

We start by describing the unforced model spin-up run to a steady state. Simulations are initialized in an ice-free state with the equilibrium line at sea level, $H_{\mathrm{ELA}} = 0$ m. Surface mass balance is therefore positive over the terrestrial portion of the bed ($r < 1000$ km), and the ice sheet begins to grow (ice sheet area jumps up initially as a thin layer of ice covers all the terrestrial part of the bed). As the ice sheet thickens, slow deformational flow expands the margin outward onto the part of the bed that is below sea level (Figure 1b), initiating ice calving into the ocean (Figure 1c). Gradually increasing ice sheet thickness (around 1100 m on average 20 kyr into the simulation) also insulates the bed and leads to warming of basal ice through geothermal heat flux. At 20 kyr in these simulations, basal sliding is initiated near the ice sheet margin in places where low till friction angle is specified. Basal ice becomes temperate, and calving at the margins of ice streams provides a significant sink of mass. Basal sliding leads to a positive feedback of frictional heating at the bed and additional meltwater production, further weakening the bed and increasing basal sliding velocity. Longitudinal stresses coupled with frictional heating at the bed then propagate this sliding 100–150 km upstream, where the bed is sufficiently warm so that frictional heating is not immediately dissipated by vertical heat conduction [*Price et al.*, 2008; *Robel et al.*, 2014]. After another 20 kyr, ice streams are fully developed and the ice sheet approaches statistical steady state (Figures 1a and 1d). Non-ice stream regions continue to expand very slowly until 120 kyr (not plotted), at which point the ice sheet volume weakly fluctuates about a statistical steady state.

3.2. Ice Sheet Response to Change in Forcing

We now apply a step change in climate forcing to the ice sheet at different times through the ice sheet growth (marked by dashed lines in Figure 1a) by increasing the ELA from 0 to 600 m uniformly over the entire

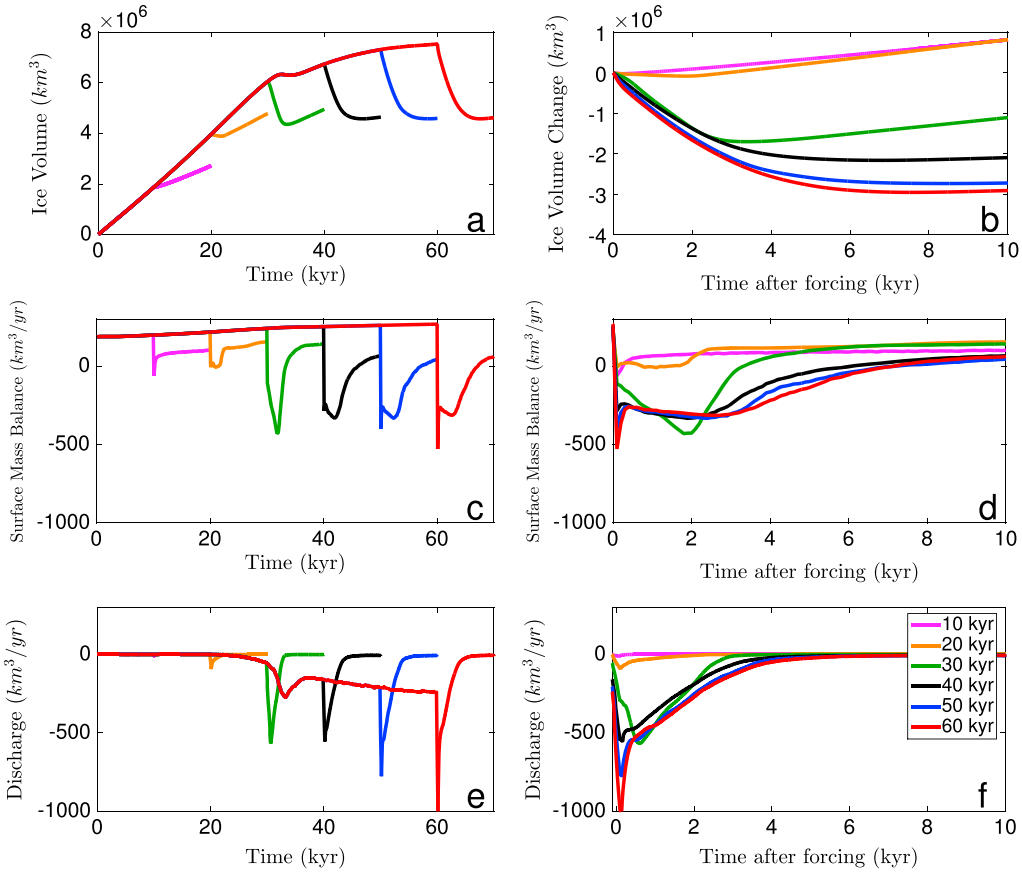

Figure 2. Ice sheet response to climate forcing at various times during growth. (a) Ice volume. (b) Change in ice volume with reference to ice volume at time of forcing. (c) Surface mass balance. (d) Surface mass balance following forcing. (e) Discharge due to calving at ice sheet margin. (f) Discharge following forcing. Figures 2e and 2f are smoothed with a 100 year window to match surface mass balance sampling rate.

domain. This change in ELA is in the range of estimated shifts in Northern Hemisphere climate resulting from Milankovitch forcing deduced from observations of snowline elevation in the modern and the last glacial period [*Andrews et al.*, 1972; *Pelto*, 1992] and used in previous model studies of last Pleistocene deglaciations [*Oerlemans*, 2002; *Pollard and DeConto*, 2005]. A more realistic simulation of deglaciation would require a fully coupled climate and surface mass balance model forced by orbital variations in Northern Hemisphere insolation, beyond the scope of our idealized process study. Nonetheless, our approach reproduces the magnitude of increased low-elevation surface melting simulated by climate models [*Carlson et al.*, 2009; *Ullman et al.*, 2015].

Figure 2 shows the ice sheet response, with each line representing a change in climate forcing at a different time (every 10 kyr). The exact timing of these changes in forcing is not meant to be compared to real Milankovitch forcing but rather to compare the response of ice sheets at different stages of ice stream development. In the simulations with step forcing applied to a large ice sheet with developing or fully developed ice streams (the green, black, blue, and red lines in Figure 2), there is a rapid decrease in ice volume in the 4 kyr following the change in forcing (Figures 2a and 2b). In small ice sheets without ice streams (magenta and orange lines in Figure 2), the climate forcing leads to a slower decrease in ice volume or a temporary slowdown in ice sheet growth but does not cause a rapid decrease in ice volume as in large ice sheet with ice streams.

The deglacial ice volume loss is decomposed into contributions due to surface mass balance (Figures 2c and 2d) and due to discharge (Figures 2e and 2f). The step change in ELA directly increases surface melting (negative surface mass balance) in all simulations (Figure 2c), followed by a recovery toward positive mass balance as the ice sheet retreats from low elevations. The temporary slowdown in ice volume growth in simulations with forcing applied to a small ice sheet occurs, in part, because the ice volume is still near or below the new equilibrium ice volume (corresponding to the changed climate) when the forcing is applied and the

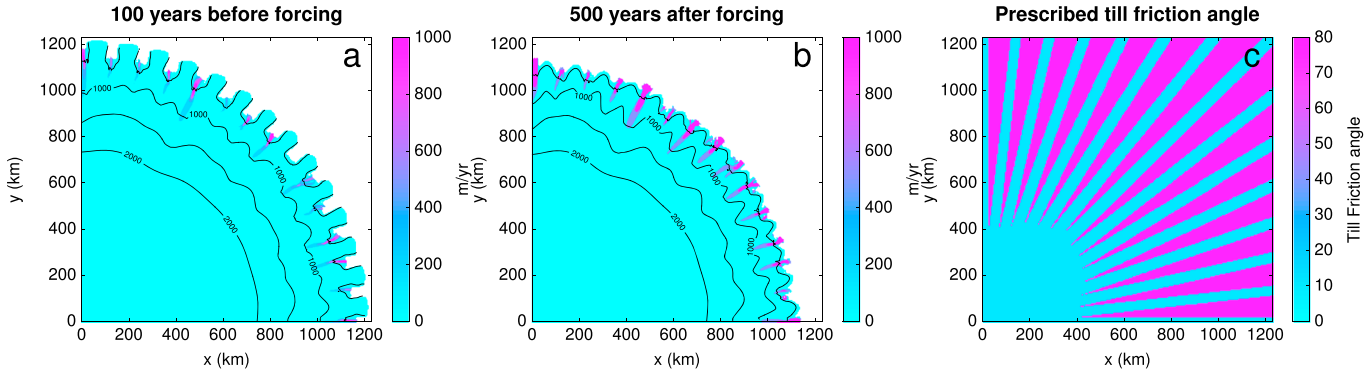

Figure 3. Snapshots of basal velocity (filled color) and ice thickness (black contours, plotted every 500 m and labeled at 1000 and 2000 m) over upper right quadrant of model domain (a) 100 years before the applied change in forcing (50.9 kyr) and (b) 500 years after the applied change in forcing (60.5 kyr). (c) Prescribed till friction angle corresponding to this simulation.

response is driven almost entirely by surface melting. However, in simulations where the change in climate forcing is applied to a large ice sheet, it is discharge due to calving at the margin (Figure 2e) which dominates the rate of deglaciation in the 3 kyr following that change. Additionally, as change in forcing is applied later in ice sheet development, the speed of the ice volume response continues to increase (Figure 2f). We conclude that as ice streams become more developed (as indicated by the magnitude of discharge), the rate of deglaciation in response to climate forcing becomes faster.

After this enhanced discharge diminishes, surface melting takes over as the primary source of mass loss (Figure 2c). This change is primarily the result of ice streams retreating from the marine portion of the bed onto the continent, where ice flux must be balanced by surface melt rather than calving. In section 4, we discuss the correspondence of this change from discharge- to surface melt-mediated deglaciation to observations.

3.3. Ice Stream Acceleration

The large increase in discharge due to calving at the margins following the prescribed change in surface mass balance (Figures 2e and 2f) is intriguing and suggests a role for ice stream dynamics. In this section we analyze the single simulation denoted by the red line in Figure 2, where the change in forcing is applied at 60 kyr. Figure 3 shows snapshots of ice sheet basal velocity and thickness just before the change in forcing and 500 years after. It is clear that ice stream velocity increases dramatically in response to the change in forcing. Figure 4 shows basal velocity and driving stress in weak till regions averaged over radial angle around the circular ice sheet and then plotted as a function of radial distance upslope from the margin and time since the change in forcing. Before the change in forcing, the ice stream onset zone is 100–150 km upstream of the margin with streaming velocities of 300–500 m/yr at the margin (yellow shading for $t < 0$ in Figure 4a), and with driving stresses of approximately 50 kPa (Figure 4b). After the forcing is changed, driving stresses in the ice stream onset zone increase (dark red shades in Figure 4b). Longitudinal stresses coupled with basal frictional heating (similar to the mechanism discussed by *Price et al.* [2008] and *Robel et al.* [2014]) then propagate the increased driving stress upstream within 2 kyr. The frictional basal heating weakens till upstream and extends the ice stream onset zone to 300–400 km upstream of the margin, where driving stresses are now 60–70 kPa. The higher driving stresses in the onset zone are accompanied by faster ice stream velocities throughout the ice stream [*Kamb and Echelmeyer*, 1986], including higher velocities near the margin of 700–1200 m/yr. The ice stream acceleration persists for 4 kyr following the change in climate forcing.

The ice stream acceleration seen here is a consequence of the dependence of the surface mass balance on elevation. In thick continental ice sheets, surface mass balance becomes more positive with elevation due to the reduction in surface melting dominating the reduction in accumulation and then saturates and does not change further with height (at H_R in equation (3)). In the simulation analyzed here, the region upstream of the ice stream in the central ice dome begins at an elevation of about 1000 m, significantly above this elevation of saturation (12 m above sea level, prior to the change in forcing), and therefore undergoes little to no change in surface mass balance due to the prescribed upward shift of the ELA (open circles in Figure 4c). On the other hand, the low-elevation ice stream trunk areas begin above or near this elevation of saturation and end below it (crosses in Figure 4c) where surface melting increases with decreasing elevation. The result is that an upward shift in ELA causes the ice streams to thin faster than the ice dome, enhancing the ice surface slope between

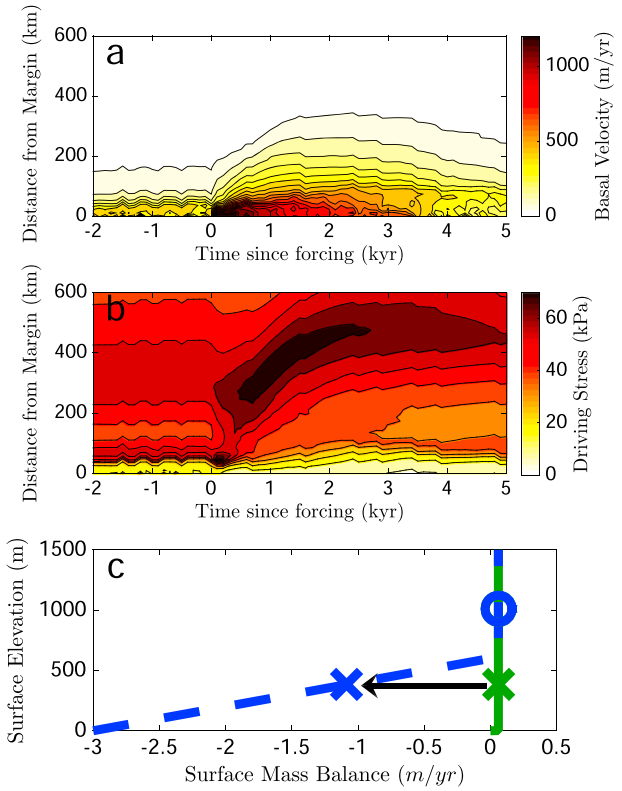

Figure 4. Mechanism of ice stream acceleration. In Figures 4a and 4b, the *x* axis is time since climate forcing and the *y* axis is the distance from ice sheet margin (radial distance upslope from margin). All quantities are averaged over radial angle with distance from the margin fixed. (a) Basal ice velocity. Lowest contoured value is 60 m/yr. (b) Driving stress. (c) Surface mass balance (SMB) changes due to change in climate forcing. Crosses indicate SMB at a typical ice stream elevation. Open circle denotes typical SMB in ice dome location, upstream of ice streams. Green line and markers indicate surface mass balance just before the change to climate forcing is applied. Blue dashed line and markers indicate surface mass balance just after.

them in the onset zone. This increases driving stress at the ice stream onset zone then leading to the simulated ice stream acceleration.

The same argument can be made mathematically using a simple mass conservation equation with a mass source $M(H)$,

$$\frac{\partial h}{\partial t} = M(H) + \frac{\partial}{\partial x}(uh), \tag{5}$$

where $H = h + b - H_{\mathrm{ELA}}$ is the ice surface elevation referenced to the ELA, h is the ice thickness, and b is the bed elevation. Differentiating with respect to x, and neglecting changes in the advective term in the time immediately after the change in climate forcing, we have an equation for the evolution of ice thickness slope

$$\frac{\partial}{\partial t}\left(\frac{\partial h}{\partial x}\right) = \frac{\partial M}{\partial x}. \tag{6}$$

Before the ELA change, $\frac{\partial M}{\partial x} = 0$ within the ice stream and at high elevation. After the upward shift in ELA, $\frac{\partial M}{\partial x}$ decreases with increasing distance from the ice dome (x), so the tendency is for surface slope to become steeper (more negative). Generally, an upward shift in ELA will yield a steepening in ice sheet surface slope where

$$\frac{\partial^2 M}{\partial H^2} < 0. \tag{7}$$

In our simulations, the presence of an elevation of saturation gives $M(H)$ negative curvature in the range of elevations corresponding to the ice stream onset regions and so results in onset steepening. It is important to note, however, that if the elevation of saturation were well above or below the elevation of ice stream onset zones, small changes in ELA would not necessarily lead to steepening.

The enhancement of discharge in non-ice stream regions as a result of the change in forcing is short lived compared to the acceleration in ice stream flux, because steepening occurs where areas of low and high ice elevation are adjacent. For ice streams this occurs in onset regions, while in non-ice stream regions this only occurs near the margins. This implies that enhanced driving stresses resulting from an upward shift in the ELA are limited to a narrower region near the ice margin in non-ice stream regions, where the response is less strong as they must contend with a strong bed which only allows slow ice flow through deformation.

3.4. The Role of Ice Streams in Ice Sheet Deglaciation

We next show how ice stream acceleration leads to rapid deglaciation through increased ice stream discharge at the margin and, to a lesser degree, due to increased surface melting in ice stream areas. We again focus on the single simulation denoted by the red line in Figure 2, where the change in forcing is applied at 60 kyr.

Total discharge is decomposed (Figure 5a) into ice stream discharge, in locations where basal velocity is over 100 m/yr (blue line), and non-ice stream discharge (green line). Following the change in forcing, there is a spike in discharge at the ice sheet margins. In ice stream regions, discharge is elevated over preforcing levels for 3 kyr following the change in forcing and remains a significant source of mass loss compared to surface mass

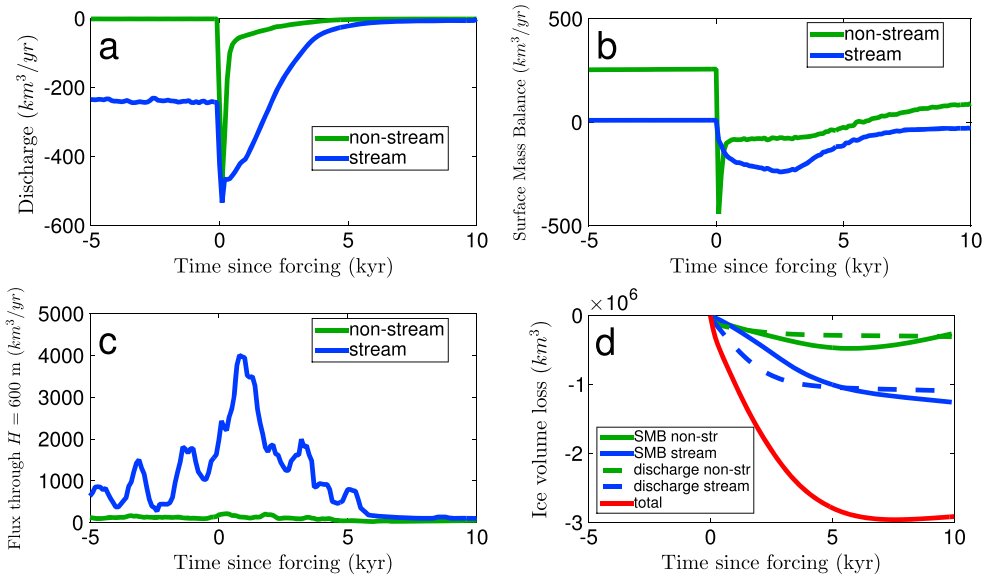

Figure 5. Decomposition of ice sheet diagnostics into ice stream and non-ice stream components. (a) Contribution to mass balance by discharge due to calving following forcing. (b) Surface mass balance following forcing. (c) Ice volume flux through the $H = 400$ m elevation contour following forcing. (d) Ice volume loss following forcing decomposed into components due to surface mass balance in non-ice stream regions (green solid line), surface mass balance in ice stream regions (blue solid line), discharge from non-ice stream regions (green dashed line), discharge from ice stream regions (blue dashed line), and the total mass loss (red line). In all panels green line is in nonstreaming regions defined as basal velocity less than 100 m/yr, and blue line is in streaming regions defined as basal velocity greater than 100 m/yr.

balance (Figure 5b) until about 5 kyr after the change in forcing. Non-ice stream margins become terrestrial and stop calving quickly following the forcing change, while ice stream margins remain marine terminating until about 6 kyr due to the flux of ice from upstream.

Ice streams also contribute to deglaciation through their contribution to the surface melting. After the step change in surface mass balance resulting from the prescribed change in the ELA, surface mass balance in ice stream regions continues to decrease and becomes more negative for 3 kyr. The continued response of surface mass balance in ice stream areas is the result of (1) upstream expansion of ice streams which brings more of the ablating ice sheet area into the ice streaming region and (2) increasing ice flux from accumulation regions to the ablation zone (Figure 5c). Thus, there is a significant part of the surface melting that can be attributed to a change in ice stream dynamics.

Figure 5d shows that total discharge accounts for more than half of all the ice volume lost during the first 4 kyr of deglaciation in this simulation, with discharge through ice streams (blue dashed line) accounting for most of the initial rate of rapid deglaciation. Not until 5 kyr after the change to climate forcing does ongoing surface melting in low-elevation ice stream regions (blue solid line) overtake discharge as the source of the majority of volume loss during deglaciation.

3.5. Robustness of Deglacial Ice Stream Acceleration

To test the robustness of our proposed mechanism to the temporal structure and time scale of the specified change in forcing, we perform a series of simulations starting after 60 kyr of ice sheet growth (red line in Figure 2) and then slowly increasing ELA, along a sinusoid, from a baseline to the same maximum as in previous simulations (600 m) and then back to the baseline (Figure 6a), meant to resemble a single Milankovitch cycle. The ice sheet response is shown in Figure 6 and compared to the step forcing simulation discussed previously (red line). In all simulations there is still an enhancement of ice stream discharge rate (Figure 6c), though it is spread out over a longer time period. When forcing is rapid (red and magenta lines), the acceleration of ice stream discharge is largest (100–300%). In addition to the peak magnitude of accelerated ice stream discharge, the duration over which ice stream discharge is maintained is equally important to determining the total contribution of ice stream discharge to deglacial ice volume loss. When forcing is slower (blue and green lines), corresponding to precession (20 kyr) and obliquity (40 kyr) cycles, the enhancement of discharge over preforcing values is smaller (30–70%) but is maintained over 8–12 kyr due to the slower retreat

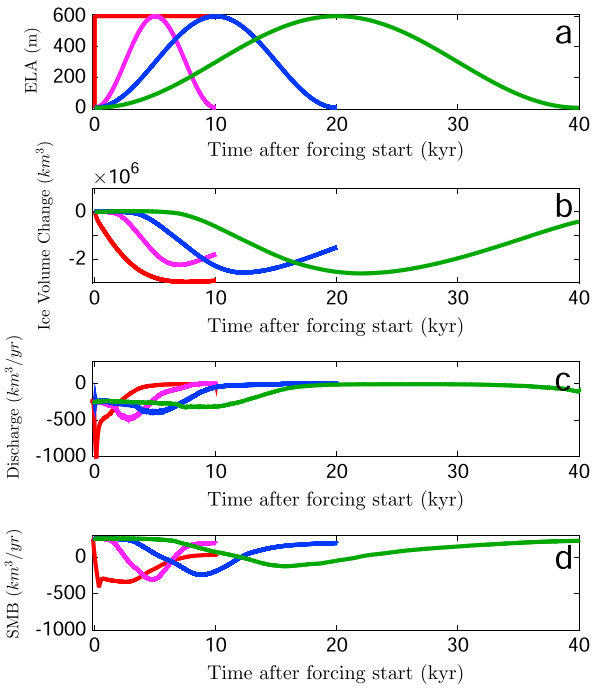

Figure 6. Ice sheet response in simulations with differing rates of changing climate forcing. (a) Specified equilibrium line altitude. (b) Change in ice volume following start of forcing change. (c) Discharge due to calving at the ice sheet margin following start of forcing. (d) Surface mass balance following start of forcing change. All curves in Figure 6c and 6d are smoothed with a 500 year filter from raw model output to eliminate numerical noise.

of ice streams from the marine portion of the bed. Regardless of the time scale of forcing, ice stream discharge results in about the same total ice volume loss over the first 5 kyr following the start of forcing. The slow acceleration and maintenance of ice stream discharge in the 20 kyr simulation (blue line) also corresponds more closely to the evolution of ice stream discharge estimated from observations by *Ullman et al.* [2015].

We have also tested the robustness of the simulated ice sheet response to horizontal model grid spacing (section S1 in the supporting information). In simulations with horizontal grid spacing near to or coarser than 20 km, ice volume loss during deglaciation is small or absent entirely. Higher resolution simulations ($\lesssim$10 km) capture ice stream width, grounding zones, and lateral viscous shear stresses. Higher ice stream discharge draws down ice thickness near the margins and produce an ice sheet more susceptible to upward shifts in the ELA. Higher-resolution simulations also capture a qualitatively similar rapid acceleration in ice stream discharge. The modeled deglaciation converges in simulations with horizontal grid spacing of less than 5 km. At high resolution, ice stream discharge is captured by the model, and the basal stress interpolation scheme employed by PISM at the grounding line does not exhibit significantly strong resolution dependence [*Feldmann et al.*, 2014]. Even when using viscosity enhancement parameters to tune ice sheet volume prior to deglaciation in coarse resolution simulations, the subsequent deglaciation is still considerably weaker than in high-resolution simulations.

We conclude that the extent to which ice streams accelerate depends on the time scale of the specified change in forcing and the accurate resolution of ice stream discharge by the model. Nonetheless, when ice streams are well resolved in the model and the change in climate forcing occurs on Milankovitch time scales, there is steepening in ice stream onset zones and significant deglaciation driven by sustained and enhanced ice stream discharge.

3.6. Ice Stream-Mediated Deglaciation of a Laurentide-Like Ice Sheet

The idealized ice sheet configuration used in the preceding sections allows us to control the timing and extent of ice streaming and determine the physical mechanisms responsible for deglaciation. There are some important differences with the Laurentide Ice Sheet, however, that hinder more direct comparisons between the deglaciation simulated in this idealized configuration and that deduced from observations. In this section, we reintroduce key aspects of the climatic and geographic complexity which characterize the Laurentide Ice Sheet and show that rapid deglaciation is still mediated by acceleration of marine-terminating ice streams, even in this more realistic configuration. The terrestrial portion of the bed is increased in size ($L = 2000$ km in equation (1) for $x > 0$ km) and extended to the southern and western model domain boundaries (Figure 7b) to produce an ice sheet with no marine boundary to the south and west. We do not intend to simulate the Cordilleran Ice Sheet and so add a mountain range and strong ablation zone in the western portion of the domain to limit ice sheet extent. In addition to the elevation-dependent surface mass balance, we add a meridional gradient in surface mass balance to produce an ablation zone over the southernmost ~500 km of the ice sheet. The northern portion of the domain has strong till in the continental interior and weak till strips of 80 km width radiating north, east, and west (Figure 7d), in line with observational estimates of average ice stream width of the Laurentide Ice Sheet [*Margold et al.*, 2015]. The southern part of the domain has

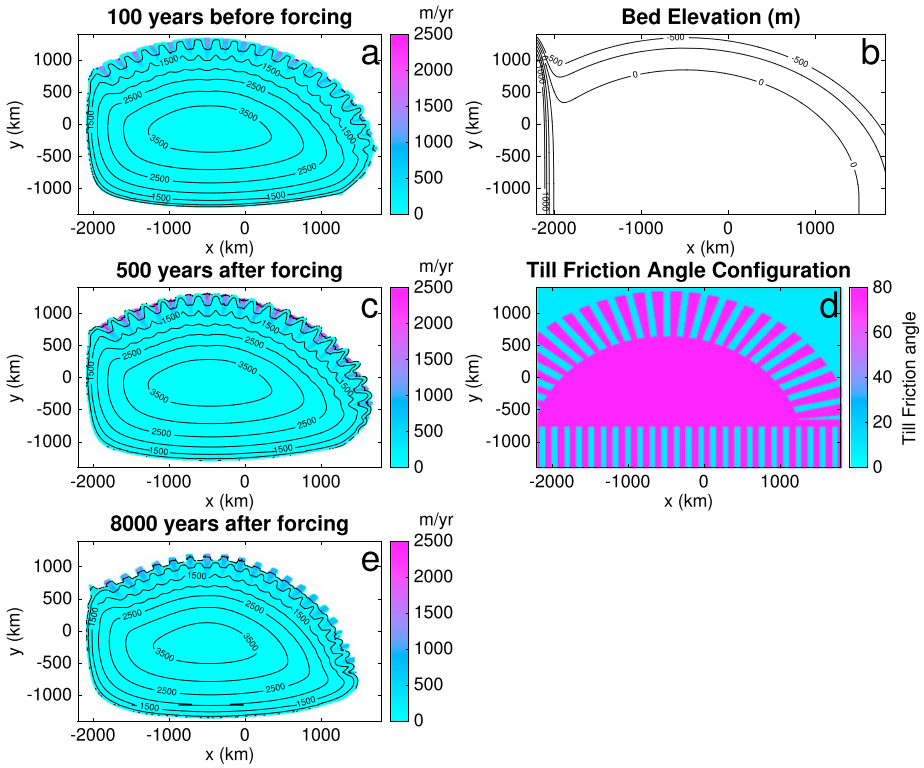

Figure 7. Snapshots and configuration from Laurentide-like ice sheet simulation. Snapshots of basal velocity (filled color) and ice thickness (black contours, plotted every 500 m and labeled at select elevations) in simulation with change in forcing applied after 40 kyr (red line in Figure 8a) (a) 100 years before the applied change in forcing, (c) 500 years after the applied change in forcing, and (e) 8000 years after the applied change in forcing. (b) Prescribed bed elevation in this simulation. (d) Prescribed till friction angle in this simulation.

weak till strips aligned in the north-south direction. There is weak till everywhere at the marine edge of the domain. This till configuration leads to the formation (Figure 7a) of marine-terminating ice streams on the northern (Arctic Ocean) and eastern (Atlantic) margins and weak (~40 m/yr sliding velocity) land-terminating ice streams at the southern margin, supported by strong surface melting at the margin, rather than calving. Overall, ice streams account for 20–25% of the ice sheet margin at the largest ice sheet extent, which is similar to the proportion of the actual Laurentide Ice Sheet that is thought to have been streaming at the LGM [*Margold et al.*, 2015]. The saturation elevation (H_R) is increased to produce higher accumulation rates at high elevations, in line with previous studies [*Cutler et al.*, 2000; *Oerlemans*, 2003; *Ullman et al.*, 2015]. These simulations are run at 10 km horizontal grid spacing due to the use of a larger domain, and all other parameters used are listed in Table 1.

The Laurentide-like ice sheet is forced with an upward shift in ELA from 0 to 600 m, after 10 and 40 kyr of ice sheet growth. As in the idealized simulations, ice streams develop over tens of thousands of years of ice sheet growth, and so when the ELA shift occurs after just 10 kyr (green lines in Figure 8), the responses in ice stream discharge and surface mass balance are relatively small and short lived, and consequently there is no deglaciation in this simulation.

When the ELA is shifted upward after 40 kyr of ice sheet growth, rapid deglaciation results. Immediately following the change in forcing, discharge through marine-terminating ice streams (Figure 7c and blue line in Figure 8b) is accelerated by 400% and remains enhanced for 5 kyr. Calving discharge at nonstreaming margins quickly diminishes as these portions of the margins retreat. Though some of the low-elevation ice streams begin below the ELA in this Laurentide-like configuration, the region upstream of onset zones is still above the ELA. Thus, the steepening mechanism described previously is still relevant for marine-terminating ice streams on the north and east margins, as ice stream onset regions experience little to no change in surface melting, while surface melting increases within ice streams. Ice streams on the north and east retreat over 10 kyr but

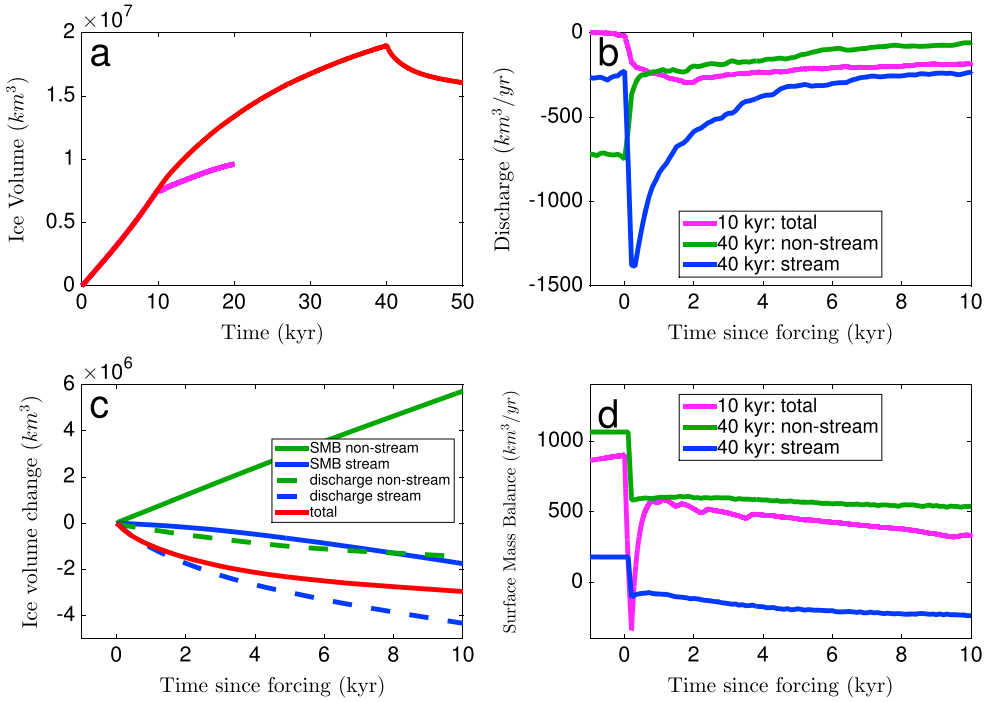

Figure 8. Ice sheet diagnostics for Laurentide-like simulations. (a) Ice volume as a function of time for simulations with change in forcing at 10 kyr (magenta line) and 40 kyr (red line). (b) Contribution to mass balance by discharge due to calving following forcing. (c) Ice volume loss following forcing in 40 kyr simulation (red line in Figure 8a) decomposed into components due to surface mass balance in non-ice stream regions (green solid line), surface mass balance in ice stream regions (blue solid line), discharge from non-ice stream regions (green dashed line), discharge from ice stream regions (blue dashed line), and the total volume change (red line). (d) Surface mass balance following forcing. In all panels green line is in nonstreaming regions defined as basal velocity less than 100 m/yr, and blue line is in streaming regions defined as basal velocity greater than 100 m/yr.

remain marine terminating, causing a slow decline in discharge and drawing down ice thickness from the interior (Figure 7e). Drawdown of interior ice thickness by marine-terminating ice streams increases the area over which surface melting occurs later in deglaciation.

In the southern ablation zone, the ELA is initially higher. Consequently, weak, land-terminating ice streams undergo considerably less steepening and less acceleration (20%) than marine-terminating ice streams in the north. However, the presence of land-terminating ice streams produces low surface elevation in the southern ablation zone, which leads to more surface melting after the change in forcing than would occur in the absence of ice streams. The southern margin does not retreat quickly following forcing, allowing land-terminating ice streams to remain active throughout deglaciation and indicating that enough ice is transported into the ablation zone to offset surface melting. Total surface mass balance remains slightly positive throughout deglaciation, with melting in low-elevation ice streams and the southern ablation zone exceeded by the continued accumulation at high elevations. The ice volume loss in the first 10 kyr of deglaciation is almost entirely dominated by discharge through marine-terminating ice streams (Figure 8c) in the northern and eastern parts of the ice sheet. However, it is possible (as shown in the convergence study in the supporting information) that simulations at even higher horizontal grid resolution would produce a larger response in ice stream discharge and deglaciation.

We conclude that a more realistic Laurentide-like ice sheet configuration undergoes deglaciation mediated, initially, by the acceleration of marine-terminating ice streams. There is increased surface melting in both streaming and nonstreaming regions, particularly in the southern ablation zone, but these changes are not large enough to drive significant ice volume loss during the early part of deglaciation. As marine-terminating ice streams in the north and east retreat and become land-terminating, surface melting over low-elevation ice streams in the south becomes the dominant driver of deglaciation.

4. Relevance to Observations and Discussion

The changes in ice stream activity during deglaciation simulated in this study are broadly consistent with ice stream changes inferred from geomorphological observations, with some differences. We have shown that accelerated ice stream discharge is the dominant source of mass loss in the early part of deglaciation following a change in surface mass balance forcing which can be caused by Milankovitch forcing. In simulations of Laurentide Ice Sheet deglaciation that are constrained by geological observations, *Stokes and Tarasov* [2010] found a similar ice stream acceleration due to increased surface slopes in onset zones, though the steepening mechanism there is not made explicit. Additionally, we show that marine-terminating ice streams, particularly those on the northern and eastern margins, initially accelerate and then slowly retreat from the marine portion of the bed and decelerate. This is broadly consistent with the geomorphological observations of ice stream activity during Laurentide deglaciation [*Shaw et al.*, 2006; *Margold et al.*, 2015], which suggest that marine-terminating ice streams decelerated during the latter half of deglaciation, once they retreated off the Arctic and Atlantic continental shelves. Our Laurentide-like ice sheet simulations do not capture the more complex spatial variations in retreat history along the Arctic and Atlantic ice sheet margins or the extent of southern margin retreat in the later part of deglaciation. These simulations lack realistic spatial heterogeneity in the prescribed topography, which does not allow for significant differences in retreat between the northern (Arctic) and eastern (Atlantic) margins. Additionally, our conservative choice of a weak climate forcing and the absence of climate feedbacks does not produce the high levels of surface melting which drives the late deglacial retreat of the southern margin deduced from observations [*Margold et al.*, 2015]. Instead, in our simulations, surface melting at the southern margin is compensated by advection of ice by land-terminating ice streams.

Stokes et al. [2016] have made a quantitative estimate of the change in ice sheet discharge during deglaciation by extrapolating ice stream velocities from geomorphological indicators of ice stream width. Though such methods do capture temporal changes in lateral shear stresses that lead to acceleration, they do not capture changes in ice stream velocity driven by driving or basal shear stress. As such, this approach precludes close, quantitative comparison to ice sheet simulations, which include all these possible drivers of ice stream acceleration.

The magnitude of idealized change in climate forcing applied here is consistent with observations of ELA change during the last deglaciation [*Andrews et al.*, 1972; *Pelto*, 1992] and previous idealized ice sheet modeling studies [e.g., *Ghil and Treut*, 1981; *Pfeffer et al.*, 1997; *Cutler et al.*, 2000; *Oerlemans*, 2003]. Other studies, such as *Abe-Ouchi et al.* [2013] and *Ullman et al.* [2015], simulated the surface mass balance of the deglaciating Laurentide Ice Sheet with a full climate model under realistic orbital forcing and found that slow surface mass accumulation at high elevation changes very little through deglaciation, while surface mass loss at low elevations increases considerably. This is consistent with the consequences of the shifted ELA on the surface mass balance in our simulations. In our slow forcing and Laurentide-like simulations (sections 3.5 – 3.6), we find that the ice stream response dominates mass balance changes during the beginning of the deglaciation, while surface mass balance only becomes negative during the later part of the deglaciation. *Ullman et al.* [2015] also argued that the first half of deglaciation must have been dominated by dynamical losses which we interpret here as the possible effect of ice stream acceleration. They find that surface mass balance (melting) can only account for the mass loss during the later parts of the deglaciation, again consistent with our findings.

In section 3.2, we show that large ice sheets with ice streams respond in a qualitatively different fashion than small ice sheets without ice streams. The precise timing of forcing in these experiments is not important, so much as the size and extent of ice stream development at those different stages if ice sheet growth. Milankovitch forcing leads to a rapid deglaciation only when the ice sheet is large and has developed ice streams. When the ice sheet is small, the same Milankovitch forcing does not result in significant deglaciation because ice streams have not yet developed (and if ice streams do not develop at all — see Figure S4 in the supporting information — the deglacial ice sheet response is considerably less). This may help explain the 100 kyr periodicity of glacial cycles over the past 700 kyr, which previous studies have attributed to a hard bed under the interior of the Laurentide Ice Sheet and the delayed development of ice streams [*Clark et al.*, 1999; *Marshall and Clark*, 2002]. It is plausible that if ice streams developed more rapidly during Laurentide Ice Sheet growth (for any number of reasons, see *Maasch and Saltzman* [1990], *DeBlonde and Peltier* [1991], *Clark and Pollard* [1998], and *Huybers and Tziperman* [2008]), deglaciations would occur every 40 kyr, as they did during the Early Pleistocene.

Our idealized modeling approach yields a strong and rapid deglaciation, even though it neglects many climatic feedbacks, which may interact with and amplify ice stream acceleration. Milankovitch variations might also result in an increase in annual mean surface temperature [*Huybers*, 2006], which could amplify the modeled deglaciation through a decrease in ice viscosity [*Licciardi et al.*, 1998]. This is confirmed by simulations (Figure S3 in the supporting information) in which we apply a uniform increase in sea level temperature (T_s in equation (4)) simultaneously with the ELA change. The result is that the early part of the simulated deglaciation of a large ice sheet is approximately 25% faster than in the ELA-only simulations discussed in the preceding sections, though the mechanism of rapid deglaciation through ice stream acceleration remains qualitatively unchanged.

Previous studies [*Oerlemans*, 1980; *Pollard*, 1982; *Abe-Ouchi et al.*, 2013] have been able to reproduce some aspects of 100 kyr glacial cycles by using coarse ice sheet models with elevation-dependent mass balance and lagged bedrock rebound. *Pollard* [1982] showed that in a simple model, parameterized calving at marine ice sheet margins contributes significantly to deglaciation and to overall agreement of simulations with the marine sediment record of glacial cycles. This is consistent with our own argument, in section 3.5, that simulations with poorly resolved ice streams have less calving and a muted deglacial response to changes in the ELA. To simulate full deglaciations without significant changes in calving associated with ice stream discharge, almost all ice sheet volume loss must then occur through increased surface melting in the margins, which requires major lowering of the bed during the late stage of glacial cycles and a significant upward shift in the ELA as a result of Milankovitch forcing (as in *Abe-Ouchi et al.* [2013]). While such high surface melting may be the sole mechanism for rapid deglaciation, our results support a combination of accelerated discharge from marine-terminating ice streams and moderate surface melting.

Inclusion of lagged bedrock rebound in a simulation of deglaciation increases surface melting in low-elevation portions of the ice sheet, while high-elevation portions of the ice sheet remain relatively unaffected by changes in ELA. In a model which resolved ice streams accurately, an increase in low-elevation melting will also lead to more steepening and ice stream acceleration. During the early part of deglaciation, a marginal increase in surface melting in low-elevation ice stream regions would likely be matched or exceeded in magnitude by the corresponding increase in ice stream discharge (barring significant changes in basal or lateral shear stress or the proportion of the ice sheet margin that is streaming), which goes like $q \propto \tau_d^3 \propto h_x^3$ [*Raymond*, 1996]. Lowering of the bed beneath ice streams could prolong the period over which ice streams remain marine terminating and active, extending the period of time over which accelerated ice streams contribute to deglaciation. Alternately, a diminishing gravitational attraction of local sea level toward retreating ice streams could act as a negative feedback (similar to *Gomez et al.* [2010]).

In our idealized bed configuration, isostatic depression leads to lowering of the entire (initially) terrestrial portion of the bed below sea level. An upward shift in the ELA then leads to unrealistically high surface melt and accelerated ice stream discharge. Thus, we have excluded isostatic depression from our simulations of deglaciation. Future work could explore the possible feedbacks between ice stream discharge and lagged bedrock rebound by including realistic bed topography in simulations of the Laurentide Ice Sheet during deglaciation.

As noted in section 2, by immediately calving all floating ice, we have removed the potential effect of buttressing ice shelves in modulating ice stream discharge. An ice shelf that provides constant buttressing to an ice stream reduces ice stream discharge. If driving stress increases far upstream of the ice shelf due to the mechanism described in this study, discharge within the grounded portion of the ice stream will increase. Longitudinal stresses then adjust to prevent large gradients in velocity at the grounding line and accommodate the newly enhanced discharge. Of course, there is also the possibility that buttressing from ice shelves may decrease during deglaciation. Previous studies have suggested that both oceanic and atmospheric warming may have caused significant ice sheet variations including Heinrich events [*Alvarez-Solas et al.*, 2010; *Marcott et al.*, 2011; *Alvarez-Solas et al.*, 2011] and Pliocene retreat of the West Antarctic Ice Sheet [*Pollard et al.*, 2015] and may play a major role in the ongoing acceleration of many Greenland and West Antarctic ice streams [*Holland et al.*, 2008; *Joughin et al.*, 2012]. However, significant uncertainty remains regarding the extent to which ice shelves buttressed large ice streams in the Laurentide Ice Sheet [*Margold et al.*, 2015]. Regardless, any ice shelf melting and reduction in buttressing that would occur in response to Milankovitch related warming would only serve to amplify the acceleration in ice stream discharge that we discuss in this study.

5. Conclusions

The main finding of this study is that enhanced discharge caused by ice stream acceleration is the primary source of ice loss during the early part of large ice sheet deglaciation in response to changes in climate forcing, such as those driven by orbital variations. This ice stream acceleration is a direct consequence of increased driving stresses in ice stream onset regions following a change in surface mass balance forcing, which is caused by a faster rate of surface melting at low ice stream elevations than at high elevations in the adjacent interior ice stream onset regions. We find that only sufficiently large ice sheets undergo such a rapid deglaciation, because ice streams are only activated once there is a sufficiently thick, marine-terminating margin and temperate basal ice. This can potentially help explain why (since the mid-Pleistocene transition) Milankovitch forcing late in a 100 kyr glacial cycle leads to full deglaciation, when the ice sheet is large and has developed ice streams, while the same forcing does not produce deglaciation early in the glacial cycle when the ice sheet is small and without ice streams. The idealized model simulations showing this ice stream acceleration and rapid deglaciation are broadly consistent with geological observations of the last deglaciation, including a greater importance of ice stream discharge early in deglaciation.

This study highlights the fact that ice flow and surface mass balance are inextricably intertwined and only when coupled together do they produce the full ice sheet response to a change in climate forcing. The acceleration in ice stream discharge discussed above is induced by a change in the surface mass balance that causes enhancement of driving stress in ice stream onset regions. In turn, ice streams play a role in determining the evolution of surface mass balance. The presence of active ice streams late in ice sheet growth produces thinner ice margins which are more susceptible to changes in climate. After a change in climate forcing, ice stream acceleration modifies the surface mass balance by rapidly transporting mass from high-elevation accumulation regions to low-elevation ablation regions. This interplay between ice flow and surface mass balance can inform the interpretation of studies which simulate deglaciation by relying on surface mass balance and neglecting ice streams.

Acknowledgments

This work has been supported by the NSF grant AGS-1303604. E.T. thanks the Weizmann Institute for its hospitality during parts of this work. A.R. has been supported by the NSF Graduate Research Fellowship. We thank Christian Schoof, Jim Rice, Jerry Mitrovica, and Richard Hindmarsh for useful suggestions and helpful conversations during the completion of this work. Special thanks go to the PISM team at the University of Alaska Fairbanks for providing timely model support. Development of PISM is supported by NASA grants NNX13AM16G and NNX13AK27G. Development of PISM is supported by NASA grants NNX13AM16G and NNX13AK27G. All model results used to produce the figures in this study are available from the corresponding author upon request from robel@caltech.edu.

References

Abe-Ouchi, A., F. Saito, K. Kawamura, M. E. Raymo, J. Okuno, K. Takahashi, and H. Blatter (2013), Insolation-driven 100,000-year glacial cycles and hysteresis of ice-sheet volume, *Nature*, *500*(7461), 190–193.

Alvarez-Solas, J., S. Charbit, C. Ritz, D. Paillard, G. Ramstein, and C. Dumas (2010), Links between ocean temperature and iceberg discharge during Heinrich events, *Nat. Geosci.*, *3*(2), 122–126.

Alvarez-Solas, J., M. Montoya, C. Ritz, G. Ramstein, S. Charbit, C. Dumas, K. Nisancioglu, T. Dokken, and A. Ganopolski (2011), Heinrich event 1: An example of dynamical ice-sheet reaction to oceanic changes, *Clim. Past*, *7*, 1297–1306.

Andrews, J., R. Barry, R. Bradley, G. Miller, and L. Williams (1972), Past and present glaciological responses to climate in eastern Baffin Island, *Quat. Res.*, *2*(3), 303–314.

Bougamont, M., P. Christoffersen, S. Price, H. Fricker, S. Tulaczyk, and S. Carter (2015), Reactivation of Kamb Ice Stream tributaries triggers century-scale reorganization of Siple Coast ice flow in West Antarctica, *Geophys. Res. Lett.*, *42*, 8471–8480, doi:10.1002/2015GL065782.

Broecker, W., and J. Van Donk (1970), Insolation changes, ice volumes, and O^{18} record in deep-sea cores, *Rev. Geophys. Space Phys.*, *8*(1), 169–198.

Broecker, W. S., and G. H. Denton (1989), The role of ocean-atmosphere reorganizations in glacial cycles, *Geochim. Cosmochim. Acta*, *53*, 2465–2501.

Budd, W., and I. Smith (1981), The growth and retreat of ice sheets in response to orbital radiation changes, *IAHS Publ.*, *131*, 369–409.

Bueler, E., and J. Brown (2009), Shallow shelf approximation as a "sliding law" in a thermomechanically coupled ice sheet model, *J. Geophys. Res.*, *114*, F03008, doi:10.1029/2008JF001179.

Calov, R., et al. (2010), Results from the Ice-Sheet Model Intercomparison Project–Heinrich Event INtercOmparison (ISMIP HEINO), *J. Glaciol.*, *56*(197), 371–383.

Calov, R., A. Ganapolski, V. Petoukhov, M. Claussen, and R. Greve (2002), Large-scale instabilities of the Laurentide Ice Sheet simulated in a fully coupled climate-system model, *Geophys. Res. Lett.*, *29*(24), 2216, doi:10.1029/2002GL016078.

Carlson, A., F. Anslow, E. Obbink, A. LeGrande, D. Ullman, and J. Licciardi (2009), Surface-melt driven Laurentide Ice Sheet retreat during the early Holocene, *Geophys. Res. Lett.*, *36*, L24502, doi:10.1029/2009GL040948.

Catania, G., C. Hulbe, H. Conway, T. Scambos, and R. CF (2012), Variability in the mass flux of the Ross ice streams, West Antarctica, over the last millennium, *J. Glaciol.*, *58*(210), 741–752.

Clark, P. U., and D. Pollard (1998), Origin of the middle Pleistocene transition by ice sheet erosion of regolith, *Paleoceanography*, *13*(1), 1–9.

Clark, P. U., R. B. Alley, and D. Pollard (1999), Northern Hemisphere ice-sheet influences on global climate change, *Science*, *286*(5442), 1104–1111.

Cutler, P. M., D. R. MacAyeal, D. M. Mickelson, B. R. Parizek, and P. M. Colgan (2000), A numerical investigation of ice-lobe–permafrost interaction around the southern Laurentide Ice Sheet, *J. Glaciol.*, *46*(153), 311–325.

Davies, J. H. (2013), Global map of solid Earth surface heat flow, *Geochem. Geophys. Geosyst.*, *14*, 4608–4622, doi:10.1002/ggge.20271.

DeBlonde, G., and W. R. Peltier (1991), A one-dimensional model of continental ice volume fluctuations through the Pleistocene: Implications for the origin of the mid Pleistocene climate transition, *J. Clim.*, *4*(3), 318–344.

Feldmann, J., T. Albrecht, C. Khroulev, F. Pattyn, and A. Levermann (2014), Resolution-dependent performance of grounding line motion in a shallow model compared with a full-Stokes model according to the MISMIP3d intercomparison, *J. Glaciol.*, *60*(220), 353–360.

Ghil, M., and H. L. Treut (1981), A climate model with cryodynamics and geodynamics, *J. Geophys. Res.*, *86*, 5262–5270.

Gildor, H., and E. Tziperman (2000), Sea ice as the glacial cycles climate switch: Role of seasonal and orbital forcing, *Paleoceanography*, *15*, 605–615.
Gildor, H., E. Tziperman, and R. J. Toggweiler (2002), Sea ice switch mechanism and glacial-interglacial CO_2 variations, *Global Biogeochem. Cycles*, *16*(3), 1032, doi:10.1029/2001GB001446.
Gomez, N., J. X. Mitrovica, P. Huybers, and P. U. Clark (2010), Sea level as a stabilizing factor for marine-ice-sheet grounding lines, *Nat. Geosci.*, *3*(12), 850–853.
Hays, J. D., J. Imbrie, and N. J. Shackleton (1976), Variations in the Earth's orbit: Pacemakers of the ice ages, *Science*, *194*, 1121–1132.
Holland, D. M., R. H. Thomas, B. De Young, M. H. Ribergaard, and B. Lyberth (2008), Acceleration of Jakobshavn Isbrae triggered by warm subsurface ocean waters, *Nat. Geosci.*, *1*(10), 659–664.
Huybers, P. (2006), Early Pleistocene glacial cycles and the integrated summer insolation forcing, *Science*, *313*(5786), 508–511.
Huybers, P., and E. Tziperman (2008), Integrated summer insolation controls 40,000 year glacial cycles in an ice-sheet energy-balance model, *Paleoceanography*, *23*, PA1208, doi:10.1029/2007PA001463.
Hyde, W. T., and W. R. Peltier (1987), Sensitivity experiments with a model of the ice-age cycle: The response to Milankovitch forcing, *J. Atmos. Sci.*, *44*(10), 1351–1374.
Jenson, J. W., D. R. MacAyeal, P. U. Clark, C. L. Ho, and J. C. Vela (1996), Numerical modeling of subglacial sediment deformation: Implications for the behavior of the Lake Michigan lobe, Laurentide Ice Sheet, *J. Geophys. Res.*, *101*(B4), 8717–8728.
Joughin, I., R. B. Alley, and D. M. Holland (2012), Ice-sheet response to oceanic forcing, *Science*, *338*(6111), 1172–1176.
Kamb, B., and K. A. Echelmeyer (1986), Stress-gradient coupling in glacier flow: I. Longitudinal averaging of the influence of ice thickness and surface slope, *J. Glaciol.*, *32*(111), 267–284.
Li, C., D. S. Battisti, D. P. Schrag, and E. Tziperman (2005), Abrupt climate shifts in Greenland due to displacements of the sea ice edge, *Geophys. Res. Lett.*, *32*, L19702, doi:10.1029/2005GL023492.
Licciardi, J. M., P. U. Clark, J. W. Jenson, and D. R. Macayeal (1998), Deglaciation of a soft-bedded Laurentide Ice Sheet, *Quat. Sci. Rev.*, *17*(4), 427–448.
Maasch, K., and B. Saltzman (1990), A low-order dynamical model of global climatic variability over the full Pleistocene, *J. Geophys. Res.*, *95*, 1955–1963.
MacAyeal, D. (1993), Binge/purge oscillations of the Laurentide Ice Sheet as a cause of the North Atlantic Heinrich events, *Paleoceanography*, *8*(6), 775–784.
Marcott, S. A., et al. (2011), Ice-shelf collapse from subsurface warming as a trigger for Heinrich events, *Proc. Natl. Acad. Sci. U. S. A.*, *108*(33), 13,415–13,419.
Margold, M., C. R. Stokes, and C. D. Clark (2015), Ice streams in the Laurentide Ice Sheet: Identification, characteristics and comparison to modern ice sheets, *Earth Sci. Rev.*, *143*, 117–146.
Marshall, S. J., and P. U. Clark (2002), Basal temperature evolution of North American ice sheets and implications for the 100-kyr cycle, *Geophys. Res. Lett.*, *29*(24), 2214, doi:10.1029/2002GL015192.
Oerlemans, J. (1980), Model experiments on the 100,000-yr glacial cycle, *Nature*, *287*(5781), 430–432.
Oerlemans, J (2002), On glacial inception and orography, *Quat. Int.*, *95*, 5–10.
Oerlemans, J. (2003), A quasi-analytical ice-sheet model for climate studies, *Nonlinear Processes Geophys.*, *10*(4–5), 441–452.
Payne, A. (1999), A thermomechanical model of ice flow in West Antarctica, *Clim. Dyn.*, *15*(2), 115–125.
Peltier, W., and S. Marshall (1995), Coupled energy-balance/ice-sheet model simulations of the glacial cycles: A possible connection between terminations and terrigenous dust, *J. Geophys. Res.*, *100*, 14,269–14,289.
Pelto, M. S. (1992), Equilibrium line altitude variations with latitude, today and during the late Wisconsin, *Palaeogeogr. Palaeoclimatol. Palaeoecol.*, *95*(1), 41–46.
Pfeffer, W., M. Dyurgerov, M. Kaplan, J. Dwyer, C. Sassolas, A. Jennings, B. Raup, and W. Manley (1997), Numerical modeling of late glacial Laurentide advance of ice across Hudson Strait: Insights into terrestrial and marine geology, mass balance, and calving flux, *Paleoceanography*, *12*(1), 97–110.
Pollard, D. (1982), A simple ice sheet model yields realistic 100 kyr glacial cycles, *Nature*, *296*, 334–338.
Pollard, D., and R. M. DeConto (2005), Hysteresis in Cenozoic Antarctic ice-sheet variations, *Global Planet. Change*, *45*(1), 9–21.
Pollard, D., R. M. DeConto, and R. B. Alley (2015), Potential Antarctic ice sheet retreat driven by hydrofracturing and ice cliff failure, *Earth Planet. Sci. Lett.*, *412*, 112–121.
Price, S., H. Conway, E. Waddington, and R. Bindschadler (2008), Model investigations of inland propagation of fast-flowing outlet glaciers and ice streams, *J. Glaciol.*, *54*(184), 49–60.
Raymond, C. (1996), Shear margins in glaciers and ice sheets, *J. Glaciol.*, *42*(140), 90–102.
Retzlaff, R., and C. Bentley (1993), Timing of stagnation of Ice Stream C, West Antarctica, from short pulse radar studies of buried surface crevasses, *J. Glaciol.*, *39*(133), 553–561.
Robel, A., C. Schoof, and E. Tziperman (2014), Rapid grounding line migration induced by internal ice stream variability, *J. Geophys. Res. Earth Surf.*, *119*, 2430–2447, doi:10.1002/2014JF003251.
Schoof, C. (2006), Variational methods for glacier flow over plastic till, *J. Fluid Mech.*, *555*, 299–320.
Shaw, J., D. Piper, G. Fader, E. King, B. Todd, T. Bell, M. Batterson, and D. Liverman (2006), A conceptual model of the deglaciation of Atlantic Canada, *Quat. Sci. Rev.*, *25*(17), 2059–2081.
Stephens, B. B., and R. Keeling (2000), The influence of Antarctic sea ice on glacial-interglacial CO_2 variations, *Nature*, *404*, 171–174.
Stokes, C., and C. Clark (2001), Palaeo-ice streams, *Quat. Sci. Rev.*, *20*(13), 1437–1457.
Stokes, C., M. Margold, C. Clark, and L. Tarasov (2016), Ice stream activity scaled to ice sheet volume during Laurentide Ice Sheet deglaciation, *Nature*, *530*(7590), 322–326.
Stokes, C. R., and L. Tarasov (2010), Ice streaming in the Laurentide Ice Sheet: A first comparison between data-calibrated numerical model output and geological evidence, *Geophys. Res. Lette.*, *37*, L01501, doi:10.1029/2009GL040990.
Tarasov, L., A. S. Dyke, R. M. Neal, and W. R. Peltier (2012), A data-calibrated distribution of deglacial chronologies for the North American ice complex from glaciological modeling, *Earth Planet. Sci. Lett.*, *315*, 30–40.
Toggweiler, J. R. (1999), Variation of atmospheric CO_2 by ventilation of the ocean's deepest water, *Paleoceanography*, *14*, 572–588.
Truffer, M., K. A. Echelmeyer, and W. D. Harrison (2001), Implications of till deformation on glacier dynamics, *J. Glaciol.*, *47*(156), 123–134.
Tziperman, E., M. Raymo, P. Huybers, and C. Wunsch (2006), Consequences of pacing the Pleistocene 100 kyr ice ages by nonlinear phase locking to Milankovitch forcing, *Paleoceanography*, *21*, PA4206, doi:10.1029/2005PA001241.
Ullman, D. J., A. E. Carlson, F. S. Anslow, A. N. LeGrande, and J. M. Licciardi (2015), Laurentide ice-sheet instability during the last deglaciation, *Nat. Geosci.*, *8*, 534–537.
Weertman, J. (1961), Stability of ice-age ice sheets, *J. Geophys. Res.*, *66*(11), 3783–3792.
Ziemen, F., C. Rodehacke, and U. Mikolajewicz (2014), Coupled ice sheet–climate modeling under glacial and pre-industrial boundary conditions, *Clim. Past*, *10*, 1817–1836.